Analyzing power in neutron-deuteron elastic scattering at $E^n_{\rm lab}$=3 MeV

J. E. McAninch,* L. O. Lamm,† and W. Haeberli
Department of Physics, University of Wisconsin–Madison, Madison, Wisconsin 53706
(Received 14 February 1994)

A measurement of the analyzing power $A_y(\theta)$ in neutron-deuteron (n-d) elastic scattering below the deuteron breakup threshold is described, including a detailed discussion of the experimental apparatus and the treatment of systematic errors. The data provide a precise test of Faddeev calculations of the three-nucleon system and of the nucleon-nucleon interaction models used as inputs to these calculations. A_y was measured at six angles from 44.5° c.m. to 145.7° c.m. to a precision of $(7\text{–}13)\times10^{-4}$. Polarized neutrons, produced by the ^{3}H$(\vec{p},\vec{n})^3$He reaction, were incident upon the target, a deuterated organic scintillator. Scattered neutrons were detected in fast coincidence with the recoil deuterons in the target. A computer simulation of the experiment was used to compensate for a number of systematic errors. Particularly important were corrections for neutron multiple scattering, accidental coincidences, and finite geometry effects. The A_y data have a 2.2% scale factor uncertainty associated with uncertainty in the polarization of the incident neutron beam. The incident neutron polarization was measured in a separate experiment using n-^{4}He scattering from a liquid helium scintillator. The neutron polarization measurement also yielded an improved value for the polarization transfer coefficient $[K^y_y(0°) = 0.650\pm0.019]$ in the ^{3}H$(\vec{p},\vec{n})^3$He reaction at $E^p_{\rm lab}$=3.80 MeV. A comparison of the A_y data to Faddeev calculations shows that the discrepancy in A_y observed previously at higher energies continues below the breakup threshold. A comparison of the A_γ data to a recent phase shift analysis of proton-deuteron (p-d) scattering indicates that observed differences between n-d and p-d analyzing powers are only partially explained by Coulomb effects.

PACS number(s): 25.10.+s, 24.70.+s, 29.25.Dz, 25.40.Dn

I. INTRODUCTION

In recent years, Faddeev calculations of the three-nucleon (3N) system have in most cases been successful in reproducing observables in the 3N bound state and in nucleon-deuteron (N-d) scattering [1,2]. One important discrepancy which has received significant attention is the observed difference between calculations and measurements of the vector analyzing power $A_y(\theta)$ in N-d elastic scattering at low energies (<50 MeV). The analyzing power A_y is consistently underestimated in both proton-deuteron (p-d) and neutron-deuteron (n-d) scattering. The size of this discrepancy is $\sim$ 25–30 % of the value of A_y near $\theta_{\rm c.m.} \approx 125°$, where A_γ has a maximum [2]. Prior to the current work, this discrepancy had been observed in n-d scattering down to $E^n_{\rm lab}$=5.0 MeV [3]. Further study of this discrepancy is of interest in that it may shed light on elements of the $3N$ and N-N systems, such as the size of three-nucleon force effects and uncertainties in the nucleon-nucleon (N-N) models used as inputs to the $3N$ calculations [1,2].

Because of difficulties encountered in neutron scattering experiments, the N-d data have traditionally been weighted toward p-d, in quantity and in precision. Calculations, on the other hand, have typically been restricted to n-d, because of difficulties encountered when including the Coulomb force. A recent exception are the p-d calculations of Berthold, Stadler, and Zankel [4] in the region below the deuteron breakup threshold ($E^N_{\rm lab}$=3.338 MeV). The importance of the Coulomb force in the p-d analyzing power has also been explored by Tornow *et al.*, [5] who used an optical model calculation to show that Coulomb force effects were of approximately the correct magnitude to account for the observed difference between the p-d and n-d analyzing powers.

The current measurements were undertaken to extend the range of precision n-d A_y data to below the deuteron breakup threshold. As an n-d measurement, the data allow comparison to 3N calculations without the need for Coulomb corrections. In addition, the data can be used to check the possibility that the A_y discrepancy could be related to an incorrect treatment of the breakup channel in 3N calculations.

In the following sections, we describe the experimental procedure and analysis. The treatment of system-

*Present address: L-397, Lawrence Livermore National Laboratory, Livermore, CA 94551.
†Present address: Physics Department, Presbyterian College, Clinton, SC 29325.

atic errors is discussed in detail. In addition, we report the measurement of the polarization transfer coefficient $K_y^y(0°)$ in the $^3\mathrm{H}(\vec{p},\vec{n})^3\mathrm{He}$ reaction at E_{lab}^p=3.80 MeV, which was performed to lower the scale factor uncertainty in the A_y data which arises from the uncertainty in the incident neutron polarization. The paper concludes with a presentation of the A_y data, which are compared to calculations based on a recent phase shift analysis of proton-deuteron (p-d) scattering.

The present measurements were previously reported [6]. As discussed in more detail below, the values reported here differ from those in Ref. [6], primarily because of the new, more accurate measurement of the polarization transfer coefficient in the neutron producing reaction.

II. APPARATUS

The measurements were made at the University of Wisconsin tandem accelerator laboratory. Polarized neutrons were produced by bombardment of tritium gas with polarized protons from a colliding-beam polarized ion source [7]. The neutrons were incident upon a target made of deuterated scintillating plastic, which served also as recoil deuteron detector. The scattered neutrons were detected in coincidence with the recoil deuterons using scintillators placed symmetrically to the left and right (Fig. 1). The polarization direction, perpendicular to the scattering plane, was reversed every 250 ms at the ion source to cancel possible systematic errors caused by left-right asymmetries in the apparatus. Coincidence n-d events were sorted according to detector (left or right) and polarization direction (up or down), and the measured analyzing power A_y was extracted from the numbers of events using the usual cross-ratio method [8]:

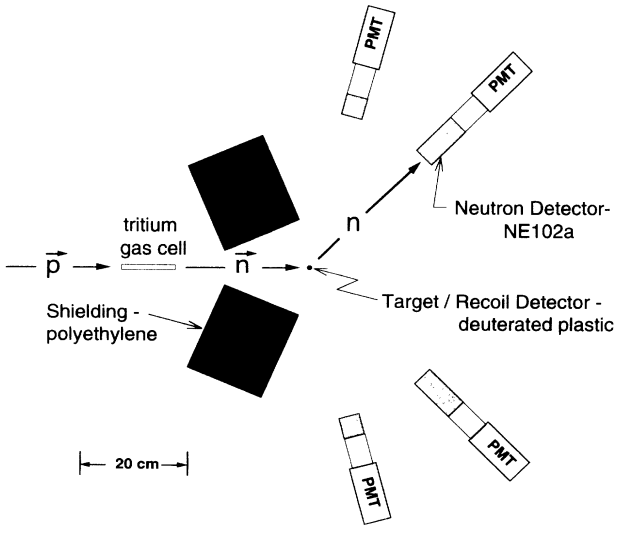

FIG. 1. Scale drawing of the apparatus.

$$A_y = \frac{\varepsilon}{p_n},$$

$$\varepsilon \equiv \frac{r-1}{r+1}, \quad r \equiv \left(\frac{N_{L\uparrow}N_{R\downarrow}}{N_{L\downarrow}N_{R\uparrow}}\right)^{1/2}, \tag{1}$$

where the N is the number of recorded scatterings and p_n is the magnitude of the neutron polarization.

The tritium gas cell consisted of a welded stainless steel tube, 1 cm diam by 10 cm long, closed at the downstream end and lined along its length with 0.1-mm-thick tantalum. The entrance foil was made of 2.5-μm-thick molybdenum. The beamstop was a gold disk, 0.5 mm thick, placed at the downstream end. The entrance foil, liner, and beamstop materials were chosen to reduce background from γ rays. The tritium cell was at room temperature, and the pressure was kept at approximately 0.9 atm, of which 0.7 atm was tritium gas. The amount of tritium was confirmed by another experimenter who measured the absolute neutron flux using neutron activation of fluorine samples placed in the neutron beam [9]. The nontritium component is assumed to be either hydrogen or deuterium. Whatever the additional gas was, no contaminant neutrons were observed.

The proton beam axis was defined by collimating slits, 5 mm wide by 10 mm high, located 1.3 m upstream of the entrance foil to the tritium cell, and a 2-mm-diam tantalum collimator, 16 cm upstream. The proton energy at the center of the tritium cell was 3.80 MeV. Neutron flux at the target was $(2\text{–}4)\times10^4$ neutrons/(s cm^2) for typical proton currents of 100–200 nA. The average energy of neutrons incident on the target was 3.01 MeV with a total spread of $\pm$0.08 MeV. The uncertainty in the proton energy was estimated to be $\pm$7 keV.

The target, which also served as recoil deuteron detector, was made of deuterated scintillating plastic.[1] The cylindrical target, 8.5 mm diam by 48.7 mm, was oriented with its axis perpendicular to the scattering plane. The diameter was chosen to strike a balance between the n-d single scattering rate and the increase in double scattering associated with a larger target. The target was cemented to a Lucite light guide, 10 mm diam by 25 mm long, which was attached to a photomultiplier tube. Because of the relatively long, thin geometry of the target, the transmission of light to the phototube tends to be nonuniform along the length of the target. The light collection efficiency was measured with a collimated beam of γ rays from a ^{60}Co source which was scanned along the length of the target scintillator. It was found that Teflon tape tightly wrapped around the target enhanced the response from the far end of the target and increased transmission. Aluminum foil, which has a lower reflectivity than Teflon tape, was used to wrap the 15 mm of the target nearest the phototube. In the final configura-

[1]Bicron BC436, purchased from the Bicron Corporation, Newbury, OH.

tion, the response varied by no more than 15% along the length of the target.

Knowledge of the atomic densities in the target was important for the calculation of the neutron multiple scattering corrections. Atomic densities were checked by comparing the measured ratio of *n-p* events to *n-d* events to the ratio calculated by the computer simulation of the experiment (see Sec. IV B). The comparison indicated that the atomic densities in the target differed significantly from the values quoted in the specification sheet. The atomic ratios given by the supplier were ^{2}H:^{1}H=20.4, (^{2}H+^{1}H):C=1.09. The simulation required a much larger hydrogen density (^{2}H:^{1}H=4.7) to reproduce the intensity of the *n-p* single scattering. The required hydrogen density was consistent for different scattering angles, even though the cross sections, neutron attenuation factors, and neutron detection efficiencies differ significantly from *n-p* to *n-d*, and vary from angle to angle.

The neutron detectors, made of NE102a scintillating plastic,[2] were 75 mm high and 40 mm wide. Four neutron detectors were used, allowing measurement of the analyzing power at two angles simultaneously. Angle pairs, in laboratory angles, were (30°, 60°), (45°, 75°), and (90°, 120°). The depth of the neutron detectors, as measured along the scattered neutron direction, was 90 mm for 30°, 45°, and 90°, and was 40 mm for 60°, 75°, and 125°. The target was placed 30 cm from the center of the tritium cell, and the front faces of the neutron detectors were placed 30 cm from the target. Root-mean-square angular acceptance was 2.2° in the laboratory.

The photomultiplier tubes were typically run at or above maximum rated voltages (~3 kV), and constant fraction discriminator levels were often set to minimum values (~3 mV). This was necessary to allow clean detection of recoils at forward angles, to maximize the efficiency of the neutron detectors at back angles, and to minimize the sensitivity to phototube gain shifts (see Sec. IV A). At these settings, pulses associated with photomultiplier dark current become significant. With RCA 8575 phototubes, noise rates of 20–100 kHz were seen, overwhelming the rates from neutrons. The rates were found to be highly sensitive to the placement of nearby conductive materials, for instance, the magnetic shielding surrounding the tube. The rates were reduced to less than 200 Hz by wrapping the phototubes tightly with aluminum foil, in direct contact with the glass. The foil was attached electrically to the photocathode pin of the tube. In addition, some of the phototubes were replaced with Hamamatsu R329-02 phototubes, which were supplied with conductive coatings.

Polyethylene shielding blocks (Fig. 1), 15 cm by 18 cm by 7.6 cm high, were placed between the tritium cell and the neutron detectors to attenuate the direct neutron flux, thereby lowering dead time in the electronics and background rates from accidental coincidences.

[2]Purchased from Thorn EMI Gencom Inc., Plainview, NY.

III. DATA ACQUISITION

Coincidences between pulses in the target and neutron detectors were collected in event mode. For each coincidence event, the integrated anode pulses in the target and neutron detector and the time delay between the pulses (the neutron time of flight) were recorded. The events were sorted off line into two-parameter histograms of recoil pulse height versus neutron time of flight (upper panel, Fig. 2) and one-parameter histograms of neutron detector pulse height. The two-parameter spectra were used to sum the *n-d* events, to separate *n-d* events from backgrounds, to measure accidental coincidence background, and for comparison to simulated spectra which were used to determine the multiple scattering background. The one-parameter (scattered neutron) spectra were used to monitor and correct for gain shifts in the neutron detector photomultiplier tubes.

For summing and gating purposes, we had the ability to set arbitrary cuts on the two-parameter spectra. Referring to the labels in the lower panel of Fig. 2, the purposes of the cuts were as follows. Cut No. 1 was used to measure the accidental coincidence background. Cuts Nos. 2–6 (shown in Fig. 7) were used to study the variation in measured analyzing power across the *n-d* peak (discussed further below). Final results were calculated

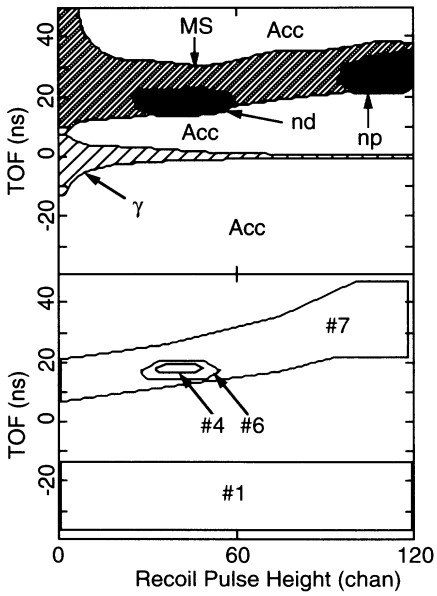

FIG. 2. Upper panel: Distribution in two-parameter spectrum (deuteron recoil pulse height vs neutron time of flight) of events taken at a laboratory angle of 60° (85.7° c.m.). Events types are the following: *nd*, neutron-deuteron single scattering; *np*, neutron-proton single scattering; MS, neutron multiple scattering background; Acc, accidental coincidence background; γ, photons. Lower panel: windows (cuts) applied to two-parameter spectra to analyze the events. Cuts Nos. 4 and 6 were used to sum the *n-d* events and to examine the variation in measured analyzing power across the *n-d* peak (see also Fig. 7). Cut No. 1 was used to measure accidental coincidence background. Cut No. 7 was used to make the projection on recoil pulse height displayed in Fig. 3.

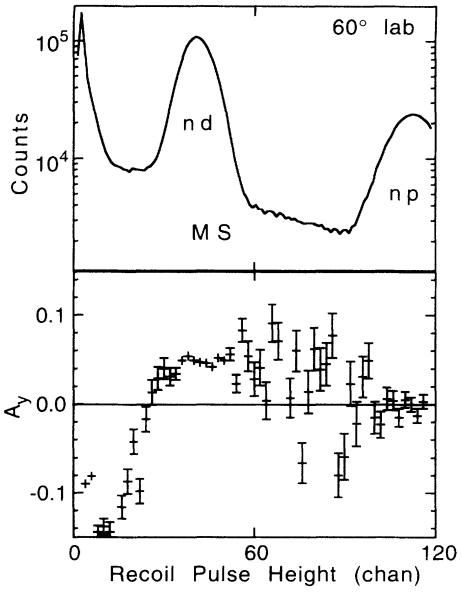

FIG. 3. Recoil pulse height spectrum for events included in cut No. 7 of Fig. 2 (60° lab). Upper panel: intensity vs recoil pulse height. Lower panel: measured analyzing power vs recoil pulse height (two-channel bins). The peaks in the spectrum correspond to *n-d* and *n-p* single scattering events, and the continuum background consists of multiple scattering events. Accidental coincidences have been subtracted from this spectrum.

from cut No. 4. A recoil pulse height spectrum (upper panel, Fig. 3), gated on cut No. 7, illustrates the relative intensities of the *n-d* and *n-p* peaks and the background continuum of multiple scattering events. Also shown (lower panel, Fig. 3) is the variation in measured analyzing power across the spectrum for the same events.

Data were taken in approximately 2 h runs with typically 50–60 runs for a given scattering angle. After correction for run-dependent effects such as accidental coincidence background and neutron polarization, the results for individual runs were compared for statistical consistency. The consistency was within expected values for all scattering angles. Reduced χ^2 values for the weighted averages were ≤ 1.11, with corresponding confidence levels ≥ 0.26, for all angles.

IV. CORRECTIONS

Special attention was given to sources of systematic errors (summarized in Table I). Significant corrections were made for accidental coincidences (Sec. IV A), finite geometry (Sec. IV B), neutron multiple scattering background and an additional, empirically determined background (Sec. IV B 1), and polarization-dependent neutron detection efficiency in the neutron detectors (Sec. IV B 2). Other corrections which were considered but determined to be less than 0.2 times the statistical uncertainty in A_y were detector dead time, possible gain shifts in neutron detectors from count rate changes associated with polarization reversal (Sec. IV A), and polarization-dependent variation in neutron flux across the scatterer [10] (Sec. IV B 3). The latter corrections are combined in Table I under the heading "other corrections."

A. Measured corrections

Corrections for accidental coincidence background and gain shifts in the neutron detector photomultiplier tubes were determined directly from the measured spectra.

Accidental coincidence events result when otherwise unrelated pulses in the target and neutron detector occur at nearly the same time (i.e., within the coincidence window). The accidental coincidence rate is approximately equal to the product of the pulse rates in the target (~20 kHz) and neutron detector (~ 20–70 kHz), and the timing window considered (~5 ns for the *n-d* peak). The variation of the accidental rate with time of flight was checked and found to be less than 5% over

TABLE I. Final results for and corrections to the analyzing power in *n-d* elastic scattering at $E^n_{\rm lab}$=3.01 MeV. These values supersede the values given in Ref. [6] for reasons given in the text. All values are in units of 10^{-2}. Laboratory angles refer to the nominal detector setting. Center of mass angles refer to the average scattering angle for detected events. Corrections are described in the text. The uncertainties listed here do not include the 2.2% scale factor uncertainty associated with the uncertainty in the incident neutron polarization. Values in parentheses give the uncertainties in rightmost digits.

Laboratory angle	30°	45°	60°	75°	90°	120°
c.m. angle	44.5°	65.8°	85.7°	104.0°	120.1°	145.7°
Corrections (10^{-2}):						
alignment uncertainty	0.000(16)	0.000(30)	0.00(2)	0.00(0)	0.00(2)	0.00(2)
accidental coincidences	−0.002(3)	−0.006(4)	−0.01(0)	−0.02(1)	0.02(1)	−0.25(1)
finite geometry	−0.011(1)	0.021(2)	0.05(0)	0.04(0)	0.02(0)	−0.01(0)
DS in target, shielding	0.280(34)	0.166(16)	0.13(2)	0.08(2)	−0.02(4)	0.01(4)
additional background	0.043(15)	−0.015(26)	0.04(2)	0.10(3)	0.00(4)	0.02(2)
polarization-dependent effect	0.042(11)	0.028(9)	−0.01(1)	−0.02(1)	−0.01(1)	0.00(0)
other corrections	−0.007(10)	−0.039(10)	−0.02(1)	−0.02(1)	0.00(2)	0.02(3)
Total correction $\Delta A_y(10^{-2})$	0.345(43)	0.155(45)	0.18(4)	0.15(4)	0.00(7)	−0.21(6)
Uncorrected results	1.160(52)	2.638(69)	4.58(10)	5.81(12)	4.74(11)	1.81(11)
Corrected results, $A_y(10^{-2})$	1.505(69)	2.793(83)	4.76(11)	5.96(13)	4.74(13)	1.60(12)

the two-parameter spectra for all scattering angles. The recoil pulse height spectrum of the accidentals was measured directly from the two-parameter spectra using cut No. 1 (lower panel, Fig. 2). Specifically, the events in cut No. 1 were used to determine the number of accidentals per two-parameter channel, as a function of recoil pulse height. Accidentals were then subtracted channel by channel from the two-parameter spectrum. Measurement and subtraction of accidentals were performed for each side (left or right) and polarization state separately, so that the polarization dependence of the background was included implicitly. Accidentals accounted for 1–5 % of the events under the *n-d* peak (cut No. 4), depending on the scattering angle.

Gain shifts in the neutron detector photomultiplier tubes change the efficiency for the detection of scattered neutrons and therefore the measured *n-d* coincidence rate, which can lead to a systematic error in the measured analyzing power when the shifts are correlated with reversal of the neutron polarization. Phototube gain shifts can be caused by variation in pulse rates. In the neutron detectors, the pulse rates are correlated to polarization reversal because the neutron production reaction has a significant analyzing power, which causes a polarization-dependent flux of background (noncoincidence) neutrons at the detectors.

Changes in the detection efficiency for scattered neutrons arise from gain shifts when pulses are "lifted" above (or "dropped" below) the threshold, as illustrated in Fig. 4. In the upper panel, events below the discriminator threshold, set at channel x_0, are not detected. (For the current measurement, 5–20 % of *n-d* events were rejected by the hardware threshold, with the larger rejection levels occurring at the back angles.) The lower panel shows the same spectrum, but with a gain shift (exaggerated for demonstration) applied. A shift in gain by a factor $(1+\delta)$ lifts some of the undetected events above threshold (solid black region), increasing the number of detected counts by $\Delta N = f x_0 \delta$, where f is the number of counts per channel in the threshold channel. The resulting polarization-dependent efficiency causes a systematic error in A_y.

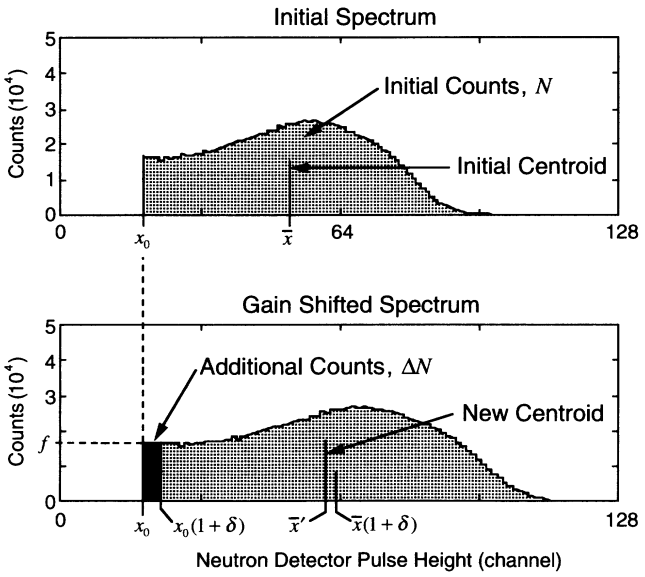

FIG. 4. Effect of a gain shift in the neutron detector photomultiplier tubes on the number N and centroid $\bar{x}$ of detected counts. The upper panel shows the spectrum of scattered neutron pulse heights for coincidence events gated by cut No. 4 of Fig. 2 (60° lab). Because of the discriminator threshold, set at channel x_0, low pulse height neutrons are not detected. The lower panel shows the same spectrum, but with a gain shift (exaggerated for demonstration) applied. A shift in gain by a factor $(1+\delta)$ lifts some of the undetected events above threshold (solid black region).

Gain shifts, and the resulting effect on A_y, were determined directly from the spectra of scattered neutron pulse heights for events gated by cut No. 4 (the *n-d* peak) of the two-parameter spectra. Gain shifts were determined by comparing the centroids of the neutron spectra for the two polarization states. The effect of a gain shift on the centroid can be seen in Fig. 4. The centroid of the unshifted spectrum (upper panel) is at channel $\bar{x}$. In the lower panel, the gain shift has moved the centroid of the *initially detected counts* (the gray region in the figure) to $\bar{x}(1+\delta)$. The centroid $\bar{x}'$ of the entire spectrum–*all detected counts*–is more complicated because of the additional low-channel counts, located at roughly $x_0(1+\delta/2)$, so that

$$\bar{x}' = \frac{N\bar{x}(1+\delta) + \Delta N x_0(1+\delta/2)}{N+\Delta N} . \qquad (2)$$

Here N is the number of counts detected without the gain shift, and the other variables are defined above.

Relative gain shifts between the two polarization states were measured to be $\delta \leq 4 \times 10^{-3}$. The resulting corrections to the measured analyzing power (included in Table I under "other corrections") were less than 20% of the statistical uncertainty in A_y at all angles.

B. Calculated corrections

A computer simulation of the experiment was used to determine corrections for systematic effects which are not directly measurable and which, because of complications inherent in neutron scattering, are not readily examined by simpler methods. Systematic effects calculated using the simulation were (a) finite geometry, (b) neutron multiple scattering in the target and shielding blocks, (c) polarization-dependent efficiency in the neutron detectors caused by neutron double scattering [11], and (d) polarization-dependent variation in the incident neutron flux across the target [10]. The calculated corrections and details of the simulation are discussed below.

1. Multiple scattering in the target and shielding

Neutron multiple scattering, primarily double scattering, is the largest and most complicated systematic error in the measurement. Multiple scattering in this context refers to events in which the neutron scatters one or more

times from nuclei in the target or other nearby materials, before or after an n-d scattering in the target (Fig. 5).

Multiple scattering events represent a background which must be subtracted from the data. The effect of a background on the measured analyzing power can be determined from Eq. (1) by adding a polarization-dependent background to the numbers of counts N. The result is

$$A^{\text{meas}} = A_y + \frac{N^{\text{bkg}}}{N^{n\text{-}d}}(A^{\text{bkg}} - A_y) \ . \tag{3}$$

Here N^{bkg} and $N^{n\text{-}d}$ are the numbers ($N \equiv N_{L\uparrow} + N_{L\downarrow} + N_{R\uparrow} + N_{R\downarrow}$) of background and n-d single scattering events, respectively, and A^{bkg} is the polarization dependence, or "analyzing power," of the background [in the sense of applying Eq. (1) to the background events]. An order-of-magnitude estimate of the effect of backgrounds (of which multiple scattering events are a significant component) can be made using Eq. (3) and the data shown in Fig. 3. Near the n-d peak, it can be estimated that $N^{\text{bkg}}/N^{n\text{-}d} \sim 5$–$10\,\%$ and that $|A^{\text{bkg}} - A_y|$ could be as large as ~ 0.10, implying a possible correction on the order of a few times 10^{-3}.

While the majority of multiple scattering events are excluded by the cuts on the two-parameter spectra, a significant number remain within the n-d peak. These remaining events are experimentally indistinguishable from n-d single scattering events. To account for this, a computer simulation of the experiment was used to estimate the intensity and polarization dependence of multiple scattering, and thereby the correction for multiple scattering. Similar calculations have been made for other experiments [10–13].

Multiple scattering is a complicated process, in that multiply scattered neutrons which reach a given detector will have undergone scatterings at a wide range of angles and from a variety of nuclei. In addition, the allowed combinations of angles and nuclei depend strongly on the geometry and other constraints (discriminator thresholds and cuts on the data) applied in the experiment. The resulting distribution and polarization dependence of detected multiple scattering events are therefore highly sensitive to these constraints, since they depend on the cross sections, analyzing powers, neutron attenuation factors, and neutron detection efficiencies involved, which themselves depend strongly on neutron energy and scattering angle. Particularly troublesome are scatterings involving carbon, present in the target and shielding blocks, because of the large n-^{12}C analyzing power, which varies rapidly with neutron energy and angle [14].

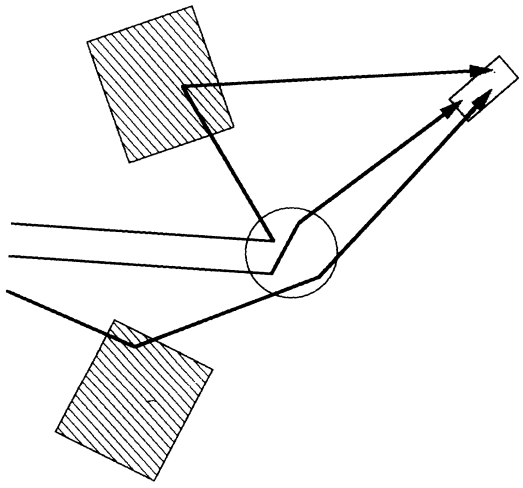

FIG. 5. Examples of detectable neutron multiple scattering events. Neutrons from the tritium gas cell enter from the left (see Fig. 1), scatter twice, and then are detected in the neutron detector. To be detected as coincidence events, there must be a detectable pulse in the neutron detector which is associated with a detectable recoil pulse in the target. This figure is not to scale.

The computer simulation performed an integration by random sampling. So that the simulation would be as realistic as possible, the following effects were included: finite geometry; finite detector resolution; neutron attenuation in the target, shielding blocks, and neutron detectors; and angle and energy dependence of differential cross sections and analyzing powers. Factors affecting the absolute intensity, such as integrated beam current, pressure in the tritium cell, and dead time in the electronics, were explicitly included as inputs to the calculation. Detector gains, discriminator threshold, and resolutions were matched to the experimental conditions, so that the simulated events were subject to the same kinematical constraints as the measured events. Sorting and binning of the simulated angle and double scattering events were identical to that of the measured events, to permit channel-by-channel subtraction of the calculated double scattering from the experimental data. The simulation covered n-d and n-p single scattering in the target and double scattering from ^{1}H, ^{2}H, and ^{12}C in the target and shielding.

Measured and simulated spectra are compared in the upper panel of Fig. 6 for events recorded at 65.8° c.m. The variation in the measured analyzing power across the spectrum is given in the lower panel. This angle was chosen for display because in many respects it is a worst case. The measured data are represented as crosses. The simulated spectra are shown as follows: simulated n-d single scattering (dash-dotted line), simulated double scattering (long dashed line), total simulated spectrum (short dashed line), additional background–discussed below (thin solid line), and simulated plus additional background (bold solid line). The shaded region shows the uncertainty in the bold solid curve.

The simulated spectra (short dashed curve in Fig. 6) accurately described the absolute intensity of n-d single scattering events (better than 5% at all angles), indicating that factors such as cross sections, neutron attenuation, detector response, and discriminator levels were well represented in the simulation. The simulation accounted for about half of the observed background in the vicinity of the n-d events. This is similar to results seen in other calculations (see, for instance, Weisel *et al.* [13]). The remaining background may be the result of a combination of triple and higher order scatterings, scatterings from nearby objects, and accumulated error in the simulation

due to uncertainties in the input cross sections and nuclear densities (see discussion of uncertainties in the simulation below). Several attempts were made to reproduce the remaining background by including additional types of events in the simulation (for instance, triple scatterings and scatterings from other nearby objects), but the effect on the simulation was small. Weisel *et al.* [13] suggested that these events may come partly from inelastic n-^{12}C scatterings in which the deexcitation γ rays are detected in the target and the associated neutrons are detected in the neutron detector. Because the incident neutron energy in the current experiment is below the first excited state of ^{12}C, this explanation is not applicable here.

To better represent the observed spectra, an empirical estimate was made of the unaccounted-for background. The assumption that this additional background has a constant analyzing power (independent of recoil pulse height) gives a reasonable representation of the observed analyzing power to the left and right of the n-d peak (bold line, bottom part of Fig. 6). The analyzing power of these additional events ($A^{\rm bkg}$) is nearly the same as the n-d analyzing power (A_y); therefore, the inclusion of this background has little effect [see Eq. (3)] on the final result. The validity of the background corrections is further discussed below.

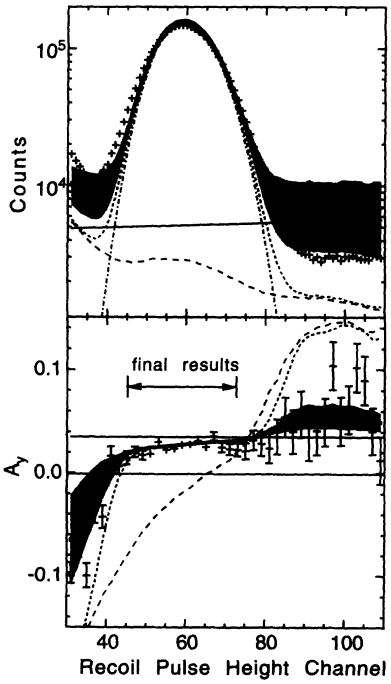

FIG. 6. Comparison of measured and calculated spectra at a laboratory angle of 45° (65.8° c.m.). Upper panel: intensity vs recoil pulse height. Lower panel: analyzing power vs recoil pulse height (two-channel bins). The measured data are represented as crosses. Curves are the following: simulated n-d single scattering (dash-dotted line), simulated double scattering (long dashed line), total simulated spectrum (short dashed line), additional background (thin solid line), and simulated plus additional (bold solid line). The shaded region shows the uncertainty in the bold solid curve. The double ended arrow marks the approximate region of events used for the final results (cuts Nos. 2–4 of Fig. 7). The agreement between calculated and measured spectra was as good or better at all other angles.

The resulting spectrum, including the simulated events and the additional background, is shown in Fig. 6 for 65.8° c.m. The bold line includes simulated single and double scattering events and the additional background (represented by the horizontal line). The shaded region indicates the estimated uncertainty (discussed below) in the simulation and additional background. The agreement between calculated and measured spectra was as good or better at all other angles.

Uncertainties in the corrections for double scattering included estimated uncertainties in the inputs to the simulation (cross sections, analyzing powers, threshold levels, etc.). The uncertainty in each data input was propagated through the calculation to determine the resulting uncertainty in the correction.

To evaluate the quality of our corrections, we compared the corrected results for A_y using different parts of the spectrum. In the tails of the n-d peak, where backgrounds dominate the spectrum, the systematic correction is dramatically increased. For a valid correction, the corrected results in the tails should agree with the results at the center of the peak. The degree of agreement therefore gives some measure of the quality of the correction. In our analysis, we performed this evaluation using the two-parameter histograms. Concentric, approximately elliptical cuts were placed on the n-d peak, roughly following its contours (Fig. 7). This provided a series of five independent "rings" of data (the areas between the contours), each of which could be analyzed separately. In the innermost cut, the ratio of background events to n-d

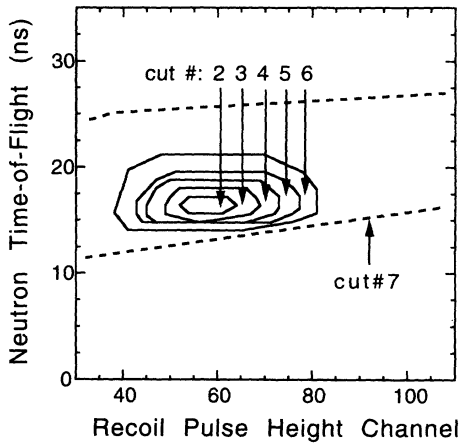

FIG. 7. "Ring" cuts applied to n-d single scattering peak in the two-parameter spectra (see also Fig. 2). The specific cuts shown were applied to the events at 45° lab (65.8° c.m.; see Fig. 6). These cuts were used to examine the variation in measured analyzing power across the n-d peak, which gives an indication of the accuracy of background corrections. In the innermost cut (No. 2), the ratio of background events to n-d events was typically 0.02, while in the outer ring (cut No. 6) the ratio was 0.5–1.5. The final results for A_y included events in cuts Nos. 2, 3, and 4.

events was typically 0.02, while in the outer ring it was 0.50–1.50.

The quality of the corrections proved to be high, in that corrected results for the five rings were statistically consistent for each angle measured. The comparison is shown in Fig. 8 for 44.5° c.m., the angle with the largest correction for a multiple scattering background. The variation in uncorrected measured analyzing power with cut is shown as open circles, which is compared to the variation expected from the calculation discussed above (solid line). The corrected values (solid diamonds) were statistically consistent–the total χ^2 for the five points was 2.66 for a confidence level of 62%–even though the correction for backgrounds for cut No. 6 was over 20 times larger than the corrections for cuts Nos. 2 and 3. This χ^2 result does not include uncertainties in the background corrections (which would lower the χ^2 result). For the final A_y data (Table I), events in cuts Nos. 2, 3, and 4 were included. This choice was made as a compromise between increased statistical uncertainty caused by using a smaller subset of the events, and increased systematic correction and uncertainty caused by using a larger subset.

Double scattering contributed 2–4% of the intensity in the n-d peak of the simulated spectra. Typically three-quarters of these events involved target nuclei only, with the remaining events involving one scattering in the shielding blocks. However, because of a larger polarization dependence in the latter events ($|A^{\rm bkg}|$ as large as 0.9 at some angles), the two event types led to approximately equal corrections to A_y. Similarly, increased polarization dependence at forward n-d angles led to a larger correction. The additional, empirically determined background contributed up to 3% of the intensity in the n-d peak, but, as stated above, its polarization dependence ($|A^{\rm bkg}| < 0.05$) was similar in magnitude to that of the n-d events, and so the associated correction to A_y was typically less than one-fifth the size of the correction for the simulated double scattering events.

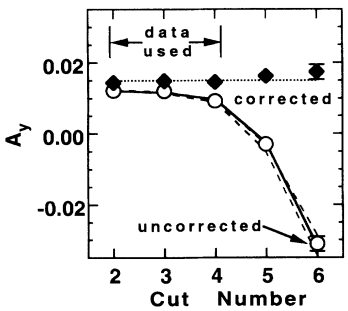

FIG. 8. Variation in measured A_y across the n-d peak at 30° lab (44.5° c.m.). Cuts are similar to those shown in Fig. 7. The measured variation in uncorrected A_y (open circles) is compared to the expected variation (solid line) and its uncertainty (dashed lines) as determined from the simulated spectrum and the additional, empirically determined background. The corrected values (solid diamonds) and their weighted average (dotted line) are also shown. The consistency in corrected values gives an indication of the accuracy of the corrections (see text). Final A_y results included the data in cuts Nos. 2, 3, and 4.

2. *Polarization-dependent neutron detection efficiency*

Double scattering (specifically, double scatterings in which an n-^{12}C scattering is followed by an n-p scattering) in the neutron detectors causes a polarization-dependent neutron detection efficiency, as first pointed out by Holslin *et al.* [11]. For the present measurement, double scattering events in the neutron detectors accounted for 13–19% of detected n-d events, as calculated by the computer simulation. For the most forward angle, the detection efficiency for these double scattering events varied by approximately 0.4% between the two polarization states, while the variation was less than 0.1% at the four back angles. The resulting corrections to A_y were significant only at the two most forward angles (see "polarization-dependent effect," Table I).

The effect of double scattering in the neutron detectors is proportional to the polarization of the neutron beam which is incident on the detectors. Knowledge of the polarization of scattered neutrons in n-d is therefore crucial to the accurate determination of the correction. In the original presentation of the A_y data [6], the scattered neutron polarization was assumed to be equal to that of the incident neutron beam. After the publication of Ref. [6], we obtained calculations of the polarization transfer $K_y^y(\theta)$ for the ^{2}H$(\vec{n},\vec{n})^2$H reaction at $E_{\rm lab}^n$=3.0 MeV from Wita*l*a [15]. The calculations were made by solving Faddeev-like 3N integral equations using as input the Bonn B nucleon-nucleon potential [16]. The calculated K_y^y values ranged from 0.58 to 0.90. The largest change in the n-d analyzing power caused by including K_y^y is at 44.5° c.m., where K_y^y=0.58. Taking into account the polarization transfer, the systematic correction to A_y at this angle changes from $7.3\pm1.9\times10^{-4}$ to $4.2\pm1.1\times10^{-4}$–a change of approximately 0.6 times the statistical uncertainty in A_y. The uncertainty in the correction for double scattering in the neutron detectors does not include the uncertainty in the n-d polarization transfer coefficient, but this uncertainty was expected to have negligible effect.

3. *Variation in incident neutron flux across the target*

The fact that the neutron production reaction has a nonzero analyzing power at small angles leads to a systematic error in the measured n-d analyzing power as first reported by Sromicki *et al.* [10]. The ^{3}H$(p,n)^3$He analyzing power causes the neutron intensity at the target to vary linearly from left to right, and the slope of this variation changes sign with reversal of the incident proton polarization. This intensity variation combines with a second effect to create the systematic error. The second effect is a shift of the effective center of the target (i.e., the weighted center of the distribution of scattering sites in the target for detected n-d events) away from the geometric center, which is caused primarily by attenuation of the scattered neutron beam while exiting the target. The direction of this shift is toward the neutron

detector; therefore, the offset is to the left for scatterings to the left detector and to the right for scatterings to the right detector. Because of this, the effective neutron flux seen by the target varies both with polarization direction and with detector. This variation does not cancel in the calculation of the measured analyzing power [see Eq. (1)], so that

$$A^{\text{meas}} \approx A_y + \frac{p_p}{p_n}\frac{dA_{(p,n)}}{d\theta}\bigg|_{0^\circ}\frac{\langle x\rangle}{r} . \quad (4)$$

Here $A_{(p,n)}$ is the $^3\text{H}(p,n)^3\text{He}$ analyzing power; p_p and p_n are the magnitudes of the proton and neutron polarizations, respectively; r is the distance from the tritium cell to the target; and $\langle x\rangle$ is the displacement of the weighted center from the geometric center, with positive $\langle x\rangle$ implying displacement toward the respective neutron detector.

The slope of the $^3\text{H}(p,n)^3\text{He}$ analyzing power for forward angles at 3 MeV is 1.5×10^{-3}/deg (see Ref. [17]), which causes a relative variation of the neutron flux across the target of 2.5×10^{-4}/mm. The displacements $\langle x\rangle$ were determined from the computer simulation to be small (0.09–0.16 mm), primarily because of the small diameter of the target. For the present measurement, the corrections to A_y for this effect were negligible [$(4–7)\times10^{-5}$].

V. PROTON POLARIZATION

The polarization of the proton beam was measured using p-^{4}He elastic scattering at laboratory angles of $\pm112.3^\circ$. The average proton energy at the center of the polarimeter was 3.70 MeV. The polarimeter was located on a separate beam line, requiring dedicated runs to measure proton polarization. Nearly 70 such runs, at approximately 8 h intervals, were made over the course of the experiment. Relative statistical uncertainty in the individual polarization measurements was typically $\pm0.3\%$, and absolute variations with time were less than ±0.015. The average proton polarization was p_p=0.87. The p-^{4}He analyzing power was calculated from the phase shifts reported by Schwandt, Clegg, and Haeberli [18]. The relative uncertainty in the p-^{4}He analyzing power was estimated in Ref. [18] to be $\pm2.0\%$ at this energy. The same proton polarimeter was used in both the n-d analyzing power measurement and the measurement of the neutron polarization (see below); therefore, this uncertainty does not enter into n-d analyzing power results.

VI. NEUTRON POLARIZATION AND K_y^y IN $^3\text{H}(\vec{p},\vec{n})^3\text{He}$

The neutron polarization was measured in a separate experiment using n-^{4}He elastic scattering. The measurement was made simultaneously at n-^{4}He laboratory angles of 54.0° and 120.5°, where the n-^{4}He analyzing power [19] is −0.452 and +0.960, respectively, to allow tests of the systematic corrections. The techniques used in the polarization measurement were similar in most respects to those used in the measurement of the n-d analyzing power.

The target/recoil ^{4}He detector was a liquid ^{4}He scintillator on loan from Kernforschungszentrum Karlsruhe, described in Ref. [20].[3] The cylindrical scintillating cell, 40 mm diam by 50 mm high, was made of thin walled (0.3 mm) stainless steel. The bottom of the cell was a 5-mm-thick quartz window. The inside walls of the cell were coated with reflecting paint, and diphenylstilbene was evaporated onto the walls and window to shift the ultraviolet scintillation light into visible wavelengths for detection by a photomultiplier tube. The diphenylstilbene layer was 200–300 μg/cm^2 thick on the walls and 10–20 μg/cm^2 thick on the inside surface of the quartz window. The choice of wavelength shifter and its thickness is described in Ref. [21].

The neutron detectors were the same as those used for the n-d analyzing power measurement. The liquid ^{4}He target was placed 55 cm from the center of the tritium cell, and the front faces of the neutron detectors were placed 50 cm from the liquid ^{4}He target.

Because of the large mass associated with the liquid helium Dewar, it was necessary to collimate the neutron beam to reduce neutron multiple scattering. The most significant mass was the liquid helium reservoir, located immediately above the scintillating volume, which had a filled capacity of approximately 10 ℓ. The collimator was made of heavy metal (primarily tungsten). The collimator was 45 cm long, with an outside diameter of 10 cm. The bore consisted of a straight section, 2 cm diam by 23 cm long and approximately centered along the length of the collimator, with conical end sections to reduce neutron scattering from the inside surface of the bore. The collimator was located with its upstream end aligned with the center of the tritium cell. Additional polyethylene shielding (replacing the shielding blocks used in the n-d measurement) was placed around the upstream end of the collimator to reduce the direct neutron flux at the neutron detectors.

The analysis of the neutron polarization data is summarized in Table II. The corrections are similar to those described above for the n-d analyzing power measurement. The measured asymmetry ε [see Eq. (1)] was corrected for accidental coincidences and gain shifts in the neutron detectors. The nominal n-^{4}He analyzing powers at 54.0° and 120.5° were calculated from the phase shifts of Bond and Firk [19]. Average analyzing powers (A_y^{av}) were calculated using a computer simulation, including finite geometry and neutron double scattering in the target. A contribution for additional background not reproduced by the simulation, similar to that used in the n-d measurement, was also included. The neutron polarization was calculated by dividing the corrected asymmetry of the averaged analyzing power. All corrections considered in the n-d measurement were considered in

[3] In Ref. [20], the target was configured as a liquid ^{3}He scintillator. For the current measurement, the apparatus for handling ^{3}He was removed.

TABLE II. Measurement of the incident neutron polarization and the polarization transfer coefficient $K_y^y(0°)$ in the ^{3}H$(\vec{p},\vec{n})^3$He reaction at $E_{\rm lab}^p$=3.80 MeV. The analysis is explained in the text. Values in parentheses give uncertainties in the rightmost digits.

Nominal n-^{4}He scattering angle (lab)	54.0°	120.5°
Contributions to n-^{4}He asymmetry, ε		
Measured asymmetry $\varepsilon^{\rm meas}$	−0.2359(19)	0.4715(46)
Corrections		
accidental coincidences	−0.0050(1)	0.0178(3)
gain shifts in neutron detectors	0.0000(4)	0.0000(20)
Corrected asymmetry $\varepsilon^{\rm corr}$	−0.2409(19)	0.4893(50)
Contributions to the averaged n-^{4}He analyzing power		
A_y at nominal energy, angle	−0.4523(50)	0.9596(18)
Uncertainty in n-^{4}He energy (±10 keV)	0.0000(25)	0.0000(9)
Uncertainty in n-^{4}He angle (±0.25°)	0.0000(0)	0.0000(3)
Corrections		
finite geometry	0.0013(4)	−0.0027(4)
double scattering in target	0.0007(0)	−0.0356(50)
additional background	0.0062(70)	−0.0327(115)
Total correction	0.0082(70)	−0.0710(125)
Averaged analyzing power $A_y^{\rm av}$	−0.4441(90)	0.8886(127)
Neutron polarization in n-d A_y measurement		
Neutron polarization measurement (ii)		
neutron polarization $p_n^{ii} \equiv \varepsilon^{\rm corr}/A_y^{\rm av}$	0.5424(118)	0.5506(97)
proton polarization p_p^{ii}	0.8343(24)	
n-d analyzing power measurement (i)		
proton polarization p_p^i	0.8660(26)	
neutron polarization $p_n^i \equiv (p_p^i/p_p^{ii})p_n^{ii}$	0.5630(125)	
^{3}H$(\vec{p},\vec{n})^3$He polarization transfer at $E_{\rm lab}^p$=3.80 MeV		
Proton polarization p_p^{ii}, incl. ±2.0% scale uncertainty	0.8343(169)	
Polarization transfer, $K_y^y(0°) \equiv p_n^{ii}/p_p^{ii}$	0.6501(193)	

this case, and those corrections not specifically listed in Table II were determined to be insignificant.

The relative uncertainties in the calculated n-^{4}He analyzing powers, included in Table II, were taken to be ±1.1% and ±0.2% at 54° and 120.5°, respectively.[4] Also listed in Table II are uncertainties caused by uncertainties in the incident neutron energy (±10 keV) and in the n-^{4}He scattering angle (±0.25°). The uncertainties in the averaged analyzing powers were dominated, however, by uncertainties in the background correction (see below).

Significant corrections for backgrounds were applied to the n-^{4}He analyzing powers (see Table II). For the 54.0° measurement, the correction (equal to 1.4% of $A_y^{\rm av}$), was dominated by the additional, empirically determined background (i.e., background not reproduced by the computer simulation). As in the n-d measurement, the intensity and analyzing power of this background was estimated from the two-parameter spectra. However, because of the poor resolution of the ^{4}He scintillator at these recoil energies, it was difficult to estimate the polarization dependence of the additional background from the outer cuts. The uncertainty in the correction for this background was therefore the dominant uncertainty in the determination of the neutron polarization in the 54.0° measurement. The total relative uncertainty in the $A_y^{\rm av}$, determined by adding in quadrature the contributing uncertainties listed in Table II, was ±2.0% for 54.0° and ±.1.4% for 120.5°.

Much larger corrections for backgrounds were applied to the measurement at 120.5°. This can be loosely understood in terms of Eq. (3) by considering the angle dependence of the n-^{4}He differential cross section and analyzing power (see Ref. [19]). At $E_{\rm lab}^n$=3 MeV, the n-^{4}He differential cross section in the laboratory system drops rapidly from nearly 900 mb/sr at 0° to ∼100 mb/sr at $\theta_{\rm lab}$ = 90° and then levels off at ∼80 mb/sr from 100° to 180°. Furthermore, the analyzing power is generally large and negative for angles less than 80°, while it is large and positive for back angles. The double scattering background is therefore dominated by events which involve (as one of the two scatterings) forward angle scatterings with a negative analyzing power. This combined with the fact that the laboratory differential cross section is 4.5 times larger than 54.0° than at 120.5° causes a background

[4]Calculated analyzing powers and the corresponding uncertainties were tabulated in Ref. [19]. Because of questions about the exact meaning of the tabulated uncertainties (discussed in the reference), those uncertainties were multiplied by 2 for the current work (Table II).

at 120.5° which is both much larger ($N^{\rm bkg}/N^{n\text{-}^4{\rm He}}$) and much more different in analyzing power ($|A^{\rm bkg} - A_y^{n\text{-}^4{\rm He}}|$), leading to a much larger systematic error. It is also worth noting that the larger cross section at 54.0° makes up for the reduced analyzing power, so that, from a statistical standpoint, the scattering at 54.0° is a somewhat better polarization analyzer than the scattering at 120.5°.

In spite of the large corrections (2% of $A_y^{\rm av}$ for 54.0° and 8% for 120.5°), the neutron polarization results for the two angles were consistent to within 1.5%. However, since the uncertainties were dominated by uncertainties in the systematic corrections and since the corrections at the two angles came from the same source and were of the same sign (in p_n), a weighted average of the two results would probably underestimate the uncertainty in the neutron polarization. Since the total correction to $A_y^{\rm av}$ was significantly smaller at 54.0° than at 120.5°, we have chosen to use only the result at 54.0° to determine the neutron polarization and the $^3{\rm H}(\vec{p},\vec{n})^3{\rm He}$ polarization transfer coefficient.

The neutron polarization for the n-d A_y measurement (p_n^i of Table II) was calculated by scaling the neutron polarization in the polarization transfer measurement by the ratio of the proton polarizations in the two measurements. The result is $p_n^i = 0.563 \pm 0.013$. The same proton polarimeter was used in both the polarization transfer measurement and the n-d analyzing power measurement; therefore, the uncertainty in the analyzing power of the polarimeter (±0.2% relative) does not enter into the uncertainty in p_n^i. The relative uncertainty (±2.2%) in p_n^i was calculated by adding in quadrature the relative total uncertainty in the neutron polarization determined by n-^{4}He scattering (p_n^{ii}) and the relative statistical uncertainties in the two proton polarizations (p_p^i and p_p^{ii}).

The updated value of the $^3{\rm H}(\vec{p},\vec{n})^3{\rm He}$ polarization transfer coefficient at $E_{\rm lab}^p$=3.80 MeV is $K_y^y(0°) = 0.650 \pm 0.019$, where the uncertainty includes the uncertainty in the analyzing power of the proton polarimeter. This result is in good agreement with an earlier value (0.661±0.033 at 3.90 MeV) reported by Donoghue *et al.* [22].

VII. n-d A_y RESULTS

Results for the n-d analyzing power are included in Table I. The final uncertainty was calculated by adding in quadrature the statistical uncertainty and the individual systematic uncertainties. The uncertainties listed do not include the 2.2% scale factor uncertainty associated with the neutron polarization uncertainty. The values in Table I supersede the values reported in Ref. [6]. The values differ for two reasons. The current results include the recent measurement of the polarization of the incident neutron beam and therefore are larger by a factor of 1.017 than the previously reported values. In addition, the correction for polarization-dependent efficiency in the neutron detectors now includes an estimate of the scattered neutron polarization, which somewhat lowers the size of the correction at the forward angles.

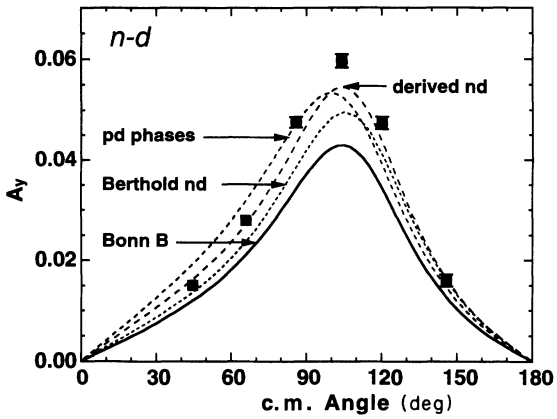

FIG. 9. The n-d analyzing power at 3.0 MeV. The solid curve is the prediction of the Bochum group using the Bonn B N-N potential model [6,15]. The remaining curves use phase shift parameters from the following sources. "Berthold, nd": (dotted line) calculated n-d phases of Refs. [4,27]. "pd phases": (short dashed line) nuclear phases of Ref. [25] (Coulomb phases set to zero). "derived nd": (long dashed line); see text.

In Fig. 9 the data are compared to theoretical predictions of the Bochum group [6] using the Bonn B N-N potential [16]. The analyzing power predictions underestimate the data by ~28% in the region of the maximum ($\theta_{\rm c.m.} \approx 105°$), similar to the discrepancy observed at higher energies. This verifies that the discrepancy is not related to the deuteron breakup channel. The predictions for A_y using the Nijmegen [23] and Paris [24] potentials are nearly indistinguishable from the Bonn B prediction (see Ref. [6]).

VIII. COMPARISON OF n-d AND p-d ANALYZING POWERS

We now compare the current n-d A_y data to the p-d data of Knutson, Lamm, and McAninch [25]. In that work p-d phase parameters at $E_{\rm lab}^p$=3 MeV extracted from a fit to p-d differential cross section data [26] and a complete set of first order p-d polarization observables (A_y, iT_{11}, T_{20}, T_{21}, and T_{22}) [25]. The phases thus obtained were compared to phase shifts determined from a momentum space Faddeev calculation of p-d observables made by Berthold, Stadler, and Zankel [4,27]. That calculation used the PEST 16 nucleon-nucleon potential [28] and included Coulomb contributions. Because of difficulties inherent in momentum space calculations, certain approximations were utilized in the treatment of the Coulomb interaction (see Refs. [4,25] for further discussion).

The comparison made in Ref. [25] showed that there was generally good agreement between the empirical and calculated p-d phases, except for significant discrepancies in the $^2S_{1/2}$ phase shift and the S-D mixing parameters. The $^2S_{1/2}$ discrepancy was presumed to be related to the

known inability of the PEST 16 potential to reproduce the ^{3}He binding energy. It was suggested that the discrepancies in the S-D mixing parameters may result from known deficiencies of the $^3S_1$-$^3D_1$ mixing in the PEST 16 potential.

For the comparison of n-d and p-d results, we examined how well the n-d data were described by the empirical p-d phase shifts, after the p-d phases had been corrected for Coulomb contributions. The Coulomb corrections were determined from the calculated phases of Berthold, Stadler, and Zankel [4,27] by taking the difference between the p-d phases, which included Coulomb contributions, and the corresponding n-d phases, which were calculated using the same N-N potential. The resulting n-d phases, derived by subtracting the calculated Coulomb corrections from the empirical p-d phases, were then used to calculate the expected n-d A_y.

The analyzing power curve calculated from the derived n-d phases is included in Fig. 9 ("derived nd," long dashed line). Two other curves are also included to show the effect of the Coulomb corrections. These were generated from the empirical p-d phases (with the proton charge set to zero) and from the Faddeev calculated n-d phases of Berthold, Stadler, and Zankel.

While the n-d phases derived from the empirical p-d phases come closer to reproducing the n-d A_y data than either of the Faddeev predictions, a discrepancy of $\sim$9% at the A_y maximum remains. This is a difference of $\sim$3 standard deviations when the scale factor uncertainty is combined with the uncertainty in the individual data point.

The remaining discrepancy indicates one (or a combination of) the following possibilities: (a) the discrepancy may be a signature of charge symmetry breaking in the 3N system; (b) the discrepancy could indicate a problem with the inclusion of the Coulomb interaction in the Faddeev calculation and the associated approximations which were involved; or (c) the discrepancy could be caused by the approach used here to make the Coulomb correction, which assumes that the effect of the Coulomb interaction on the nuclear phases is insensitive to the magnitude of the phases. The last possibility could be checked by varying the N-N potential used as input to the Faddeev calculation, with the aim of more closely reproducing the empirical p-d phases and observing the change in the difference between the n-d and p-d phases.

To further examine the remaining discrepancy, we attempted to fit the n-d A_y data and the n-d differential cross section data of Ref. [29]. Using the derived n-d phases as initial values, the $^2S_{1/2}$ and ^4P_j were allowed to vary to minimize χ^2. While significantly improved fits could be obtained, the results were mostly inconclusive because of the limited n-d data set.

IX. SUMMARY

We have presented a measurement of the n-d analyzing power $A_y(\theta)$ at $E^n_{\rm lab}$=3.0 MeV, including a discussion of the experimental procedure and analysis and the treatment of systematic errors. We also report a measurement of the polarization transfer coefficient $K^y_y(0°)$ in the ^{3}H$(\vec{p},\vec{n})^3$He reaction at $E^p_{\rm lab}$=3.80 MeV, which provided an improved calibration of the neutron polarization for the A_y data.

The A_y data represent the first precision measurement of the n-d analyzing power below the deuteron breakup threshold. The data are significantly underestimated by theoretical calculations of the 3N system using modern nucleon-nucleon potential models, similar to discrepancies seen at higher energies. A comparison of the n-d A_y data to p-d data taken at the same energy showed that available Coulomb corrections were not sufficient to account for the observed difference between the n-d and p-d analyzing powers.

ACKNOWLEDGMENTS

The authors wish to thank Dr. W. Glöckle, at the Ruhr-Universität, Bochum, and Dr. H. Witała, at Jagellonian University, Cracow, for providing their calculations of n-d observables. We wish to thank Dr. H. O. Klages, at the Kernforschungszentrum Karlsruhe, for the loan of the liquid helium target and neutron collimator. We are grateful to T. Finnessy for his invaluable assistance in maintaining the ion source and accelerator, in setting up experimental apparatus, and during the measurement. This work was supported in part by the United States National Science Foundation.

[1] I. Slaus and A. Marušić, Nucl. Phys. **A543**, 213c (1992).
[2] H. Witała and W. Glöckle, Nucl. Phys. **A528**, 48 (1991), and references therein.
[3] W. Tornow, C. R. Howell, M. Alohali, Z. P. Chen, P. D. Felsher, J. M. Hanly, R. L. Walter, G. Weisel, G. Mertens, I. Slaus, H. Witała, and W. Glöckle, Phys. Lett. B **257**, 273 (1991).
[4] G. H. Berthold, A. Stadler, and H. Zankel, Phys. Rev. C **41**, 1365 (1990); Phys. Rev. Lett. **61**, 1077 (1988).
[5] W. Tornow, C. R. Howell, R. L. Walter, and I. Slaus, Phys. Rev. C **45**, 459 (1992).
[6] J. E. McAninch, W. Haeberli, H. Witała, W. Glöckle, and J. Golak, Phys. Lett. B **307**, 13 (1993); J. E. McAninch, Ph.D. thesis, University of Wisconsin-Madison, 1993, available from University Microfilms, Ann Arbor, MI 48106.
[7] W. Haeberli, M. D. Barker, C. A. Gossett, D. G. Mavis, P. A. Quin, J. Sowinski, T. Wise, and H. F. Glavish, Nucl. Instrum. Methods **196**, 319 (1982).
[8] R. C. Hanna, in *Proceedings of the 2nd International Symposium on Polarization Phenomena of Nucleons*, edited by P. Huber and H. Schopper (Burkhäuser Verlag, Basel, 1966), p. 280.
[9] C. Hartmann (personal communication).
[10] J. Sromicki, D. Holslin, M. D. Barker, P. A. Quin, and W. Haeberli, Phys. Rev. Lett. **57**, 2359 (1986).

[11] D. Holslin, J. McAninch, P. A. Quin, and W. Haeberli, Phys. Rev. Lett. **61**, 1561 (1988); D. Holslin, J. McAninch, J. Sromicki, P. A. Quin, and W. Haeberli, Nucl. Instrum. Methods A **274**, 207 (1989).
[12] W. Tornow, P. W. Lisowski, R. C. Byrd, and R. L. Walter, Nucl. Phys. **A340**, 34 (1980).
[13] G. J. Weisel, W. Tornow, C. R. Howell, P. D. Felsher, M. AlOhali, Z. P. Chen, R. L. Walter, J. M. Lambert, P. A. Treado, and I. Slaus, Phys. Rev. C **46**, 1599 (1992).
[14] R. J. Holt, F. W. K. Firk, R. Nath, and H. L. Schultz, Nucl. Phys. **A213**, 147 (1973), and references therein.
[15] H. Witała (private communication).
[16] R. Machleidt, Adv. Nucl. Phys. **19**, 189 (1989).
[17] J. R. Smith and S. T. Thornton, Nucl. Phys. **A186**, 161 (1972).
[18] P. Schwandt, T. B. Clegg, and W. Haeberli, Nucl. Phys. **A163**, 432 (1971).
[19] J. E. Bond and F. W. K. Firk, Nucl. Phys. **A287**, 317 (1977).
[20] R. van Staa, J. Reher, and B. Zeitnitz, Nucl. Instrum. Methods **136**, 241 (1976).
[21] J. Reher, diploma work, University of Hamburg, 1976.
[22] T. R. Donoghue, R. C. Haight, G. P. Lawrence, J. E. Simmons, D. C. Dodder, and G. M. Hale, Phys. Rev. Lett. **27**, 947 (1971); R. C. Haight, J. E. Simmons, and T. R. Donoghue, Phys. Rev. C **5**, 1826 (1972).
[23] M. M. Nagels, T. A. Rijken, and J. J. de Swart, Phys. Rev. D **17**, 768 (1978).
[24] M. Lacombe, B. Loiseau, J. M. Richard, R. Vinh Mau, J. Côté, P. Pirès, and R. de Tourreil, Phys. Rev. C **21**, 861 (1980).
[25] L. D. Knutson, L. O. Lamm, and J. E. McAninch, Phys. Rev. Lett. **71**, 3762 (1993).
[26] D. C. Kocher and T. B. Clegg, Nucl. Phys. **A132**, 455 (1969).
[27] G. H. Berthold (private communication).
[28] J. Haidenbauer and W. Plessas, Phys. Rev. C **30**, 1822 (1984).
[29] P. Schwartz, H. O. Klages, P. Doll, B. Haesner, J. Wilczynski, and B. Zeitnitz, Nucl. Phys. **A398**, 1 (1983).

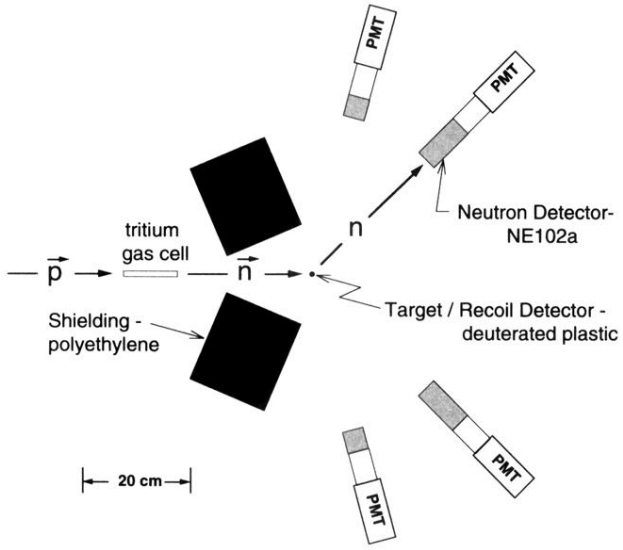

FIG. 1. Scale drawing of the apparatus.

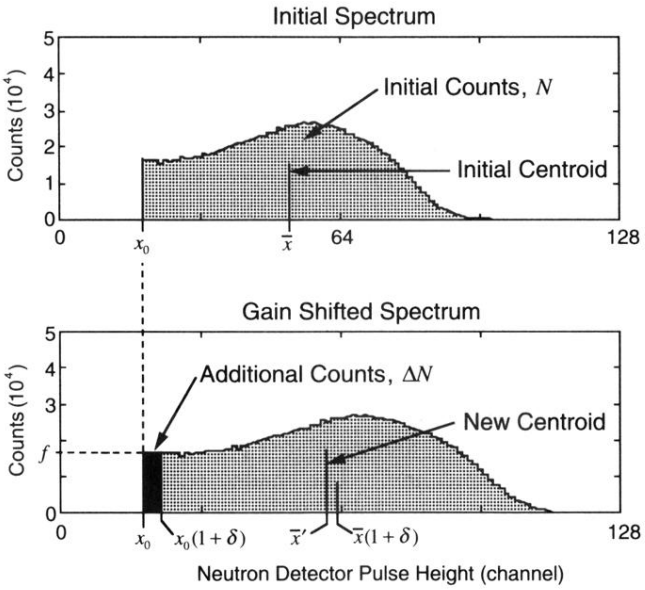

FIG. 4. Effect of a gain shift in the neutron detector photomultiplier tubes on the number N and centroid $\bar{x}$ of detected counts. The upper panel shows the spectrum of scattered neutron pulse heights for coincidence events gated by cut No. 4 of Fig. 2 (60° lab). Because of the discriminator threshold, set at channel x_0, low pulse height neutrons are not detected. The lower panel shows the same spectrum, but with a gain shift (exaggerated for demonstration) applied. A shift in gain by a factor $(1+\delta)$ lifts some of the undetected events above threshold (solid black region).

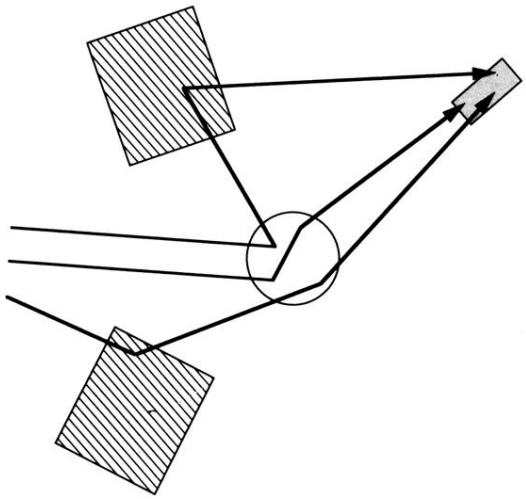

FIG. 5. Examples of detectable neutron multiple scattering events. Neutrons from the tritium gas cell enter from the left (see Fig. 1), scatter twice, and then are detected in the neutron detector. To be detected as coincidence events, there must be a detectable pulse in the neutron detector which is associated with a detectable recoil pulse in the target. This figure is not to scale.